

# SAM68 is a physiological regulator of *SMN2* splicing in spinal muscular atrophy

Vittoria Pagliarini,<sup>1,2</sup> Laura Pelosi,<sup>4</sup> Maria Blaire Bustamante,<sup>1,2</sup> Annalisa Nobili,<sup>3,5</sup> Maria Grazia Berardinelli,<sup>4</sup> Marcello D'Amelio,<sup>3,5</sup> Antonio Musarò,<sup>4,6</sup> and Claudio Sette<sup>1,2</sup>

<sup>1</sup>Department of Biomedicine and Prevention, University of Rome Tor Vergata, 00133 Rome, Italy

<sup>2</sup>Laboratory of Neuroembryology, Fondazione Santa Lucia, 00143 Rome, Italy

<sup>3</sup>Laboratory of Molecular Neuroscience, Fondazione Santa Lucia, 00143 Rome, Italy

<sup>4</sup>Institute Pasteur Cenci-Bolognietti Foundation, DAHFMO-Unit of Histology and Medical Embryology, IIM, University of Rome La Sapienza, 00161 Rome, Italy

<sup>5</sup>Medical School University Campus Bio-Medico, 00128 Rome, Italy

<sup>6</sup>Center for Life Nano Science@Sapienza, Istituto Italiano di Tecnologia, 00161 Rome, Italy

Spinal muscular atrophy (SMA) is a neurodegenerative disease caused by loss of motor neurons in patients with null mutations in the *SMN1* gene. The almost identical *SMN2* gene is unable to compensate for this deficiency because of the skipping of exon 7 during pre-messenger RNA (mRNA) processing. Although several splicing factors can modulate *SMN2* splicing in vitro, the physiological regulators of this disease-causing event are unknown. We found that knockout of the splicing factor SAM68 partially rescued body weight and viability of SMA $\Delta$ 7 mice. Ablation of SAM68 function promoted *SMN2* splicing and expression in SMA $\Delta$ 7 mice, correlating with amelioration of SMA-related defects in motor neurons and skeletal muscles. Mechanistically, SAM68 binds to *SMN2* pre-mRNA, favoring recruitment of the splicing repressor hnRNP A1 and interfering with that of U2AF65 at the 3' splice site of exon 7. These findings identify SAM68 as the first physiological regulator of *SMN2* splicing in an SMA mouse model.

## Introduction

Spinal muscular atrophy (SMA) is the leading genetic cause of infant mortality, with an incidence of approximately one in 6,000–10,000 newborns (Arnold and Burghes, 2013; Nurputra et al., 2013). SMA is an autosomal recessive neuromuscular disorder primarily characterized by degeneration of spinal cord motor neurons and consequent atrophy of skeletal muscles. The disease is most commonly caused by homozygous deletion of the *Survival Motor Neuron 1* (*SMN1*) gene, leading to reduced levels of the ubiquitously expressed SMN protein (Arnold and Burghes, 2013; Nurputra et al., 2013). SMN plays key roles in several canonical cellular pathways, including biogenesis of the small nuclear RNPs, which are core components of the spliceosome (Wahl et al., 2009), pre-mRNA splicing, and RNA transport (Li et al., 2014). Nevertheless, attempts to directly link aberrant RNA processing with SMA pathogenesis have proven controversial (Zhang et al., 2008; Bäumer et al., 2009).

SMA patients retain at least one copy of the almost identical *SMN2* gene. However, although it encodes a virtually identical protein, the expression levels of *SMN2* are not sufficient to restore full SMN activity (Arnold and Burghes, 2013; Nurputra et al., 2013). The coding regions of *SMN1* and *SMN2* differ only

for a silent C to T transition at position 6 in exon 7, leading to the skipping of exon 7 in most *SMN2* transcripts and to production of an unstable SMN $\Delta$ 7 protein that is rapidly degraded (Burnett et al., 2009; Cho and Dreyfuss, 2010). The residual low levels of *SMN2* transcripts that include exon 7 produce small amounts of fully functional SMN protein, supporting early development and viability in patients and mouse models of SMA (Arnold and Burghes, 2013; Nurputra et al., 2013). Currently, there is no cure for SMA patients (Lorson and Lorson, 2012; Arnold and Burghes, 2013). Because rescue of exon 7 splicing represents a suitable therapeutic approach for SMA, understanding the molecular mechanisms involved in the regulation of this splicing event is of fundamental importance.

Many RNA-binding proteins (RBPs) have been proposed to play a role in the regulation of *SMN2* splicing in vitro (Hofmann et al., 2000; Hofmann and Wirth, 2002; Kashima and Manley, 2003; Kashima et al., 2007; Bose et al., 2008; Chen et al., 2008; Pedrotti et al., 2010; Singh et al., 2011), including hnRNP A1 (Kashima and Manley, 2003; Kashima et al., 2007) and SAM68 (Pedrotti et al., 2010), suggesting that the relative expression levels or activity of specific splicing factors can modulate *SMN2* splicing (Pedrotti and Sette, 2010). However,

Correspondence to Claudio Sette: [claudio.sette@uniroma2.it](mailto:claudio.sette@uniroma2.it)

Abbreviations used in this paper: AChR, acetylcholine receptor; ANOVA, analysis of variance; ChAT, choline acetyltransferase; CLIP, cross-linking immunoprecipitation; CSA, cross-sectional area; dpp, day postpartum; IVS, interventricular septum; NMJ, neuromuscular junction; qPCR, quantitative real-time PCR; RBP, RNA-binding protein; SMA, spinal muscular atrophy.

© 2015 Pagliarini et al. This article is distributed under the terms of an Attribution-Noncommercial-Share Alike-No Mirror Sites license for the first six months after the publication date (see <http://www.rupress.org/terms>). After six months it is available under a Creative Commons License (Attribution-Noncommercial-Share Alike 3.0 Unported license, as described at <http://creativecommons.org/licenses/by-nc-sa/3.0/>).

whether any of these regulators play a role in vivo and contribute to the SMA phenotype is still currently unknown.

Herein, we have investigated the role of SAM68—a member of the signal transduction and activation of RNA family of RBPs (Lukong and Richard, 2003; Bielli et al., 2011)—in the regulation of *SMN2* splicing in vivo by using the SMA $\Delta$ 7 mouse model (Le et al., 2005). We show that SAM68 binds the exon 7 region of *SMN2* pre-mRNA in vivo, promoting recruitment of the splicing repressor hnRNP A1 and interfering with binding of the general splicing factor U2AF65. Ablation of SAM68 activity was accompanied by a partial recovery in body weight, viability, and motility of SMA $\Delta$ 7 mice. These effects correlated with regulation of *SMN2* splicing, as knockout of *Sam68* increased exon 7 inclusion and SMN expression in the cortex, cerebellum, spinal cord, and peripheral tissues of SMA $\Delta$ 7 mice. Recovery of SMN expression resulted in an increase in nuclear gems in spinal cord motor neurons and in reduction of motor neuron loss, leading to significant amelioration of SMA-related defects in neuromuscular junctions (NMJs), skeletal muscles, and other peripheral organs. This work provides the first evidence of a splicing factor that modulates *SMN2* splicing and SMN expression in vivo, thus affecting the phenotype of an SMA mouse model.

## Results

### SAM68 binds *SMN2* exon 7 and mediates recruitment of hnRNP A1 in vivo

In cultured cells, SAM68 binds the *SMN2*-specific exonic splicing silencer created by the C to T transition in exon 7 (UUUUA), thus repressing its recognition by the spliceosome through recruitment of the splicing repressor hnRNP A1 and causing exon skipping in transfected cells and in SMA fibroblasts in culture (Pedrotti et al., 2010). To determine whether SAM68 binds *SMN2* exon 7 also in a physiological context, we performed UV-cross-linking immunoprecipitation (CLIP) experiments in the brain of non-SMA (*SMN2 $\Delta$ 7;SMN2;Snn<sup>+/+</sup>*) mice that are either wild type (*Sam68<sup>+/+</sup>*) or knockout (*Sam68<sup>-/-</sup>*) for *Sam68*. CLIP assays were evaluated by quantitative real-time PCR (qPCR) using primers spanning the *SMN2* transcription unit (Fig. 1 A). SAM68 was recruited to the transgenic human *SMN2* pre-mRNA in the *Sam68<sup>+/+</sup>* brain, with a strong enrichment at the intron 6–exon 7 junction (I6/E7), whereas binding was reduced in the downstream junction (E7/I7) and in the upstream exons 3 and 5 (Fig. 1 B). SAM68 signals detected by CLIP assays were specific, as demonstrated by the strongly reduced or absent binding observed in *SMN2 $\Delta$ 7;SMN2;Snn<sup>+/+</sup>* mice that are knocked out for *Sam68* (*Sam68<sup>-/-</sup>*) (Fig. S1 A). Importantly, hnRNP A1 was efficiently recruited to the exon 7 region of the *SMN2* pre-mRNA in *Sam68<sup>+/+</sup>* mice, but its binding was strongly impaired in *Sam68<sup>-/-</sup>* mice (Fig. 1 C). These results suggest that binding of SAM68 to the intron 6–exon 7 junction of *SMN2* pre-mRNA favors the recruitment of a splicing repressor in a physiological context of relevance for SMA.

U2AF65 is a general splicing factor that favors assembly of the U2 small nuclear RNP to the 3' splice site (ss) and promotes exon definition (Wahl et al., 2009). Because SAM68 binds near the 3' ss of exon 7 (Fig. 1 B), we tested whether it competes with recruitment of U2AF65 by performing in vitro pull-down assays using RNA-biotinylated probes of the *SMN2* exon 7 region with the flanking 3' intron including the branch

site (Fig. 1 D; Pedrotti et al., 2010). A streptavidin pull-down assay using brain nuclear extracts showed that knockout of *Sam68* expression increased recruitment of U2AF65 to *SMN2* exon 7 RNA (Fig. 1 E). Conversely, overexpression of FLAG-SAM68 in HEK293T interfered with binding of endogenous U2AF65 to the 3' ss (Fig. 1 F).

These experiments indicate that binding of SAM68 to *SMN2* exon 7 favors the recruitment of a splicing repressor while counteracting that of a positive splicing regulator.

### Ablation of *Sam68* expression partially rescues viability, body weight, and motor function of SMA $\Delta$ 7 mice

SMA $\Delta$ 7 mice carry a homozygous deletion of the mouse *Snn* gene, two copies of the human *SMN2* transgene, and the human *SMN2 $\Delta$ 7* cDNA (*SMN2 $\Delta$ 7;SMN2;Snn<sup>-/-</sup>*; Le et al., 2005). To investigate whether SAM68 plays a role in SMA, we crossed *SMN2 $\Delta$ 7;SMN2;Snn<sup>+/+</sup>* mice with *Sam68<sup>+/+</sup>* mice (Fig. 2 A). Heterozygote mice were used because *Sam68<sup>-/-</sup>* males are sterile (Paronetto et al., 2009) and females are subfertile (Bianchi et al., 2010). Genotyping of the offspring confirmed that double knockout mice (*SMN2 $\Delta$ 7;SMN2;Snn<sup>-/-</sup>;Sam68<sup>-/-</sup>*) were born (Fig. 2 A). A backcross of heterozygote mice was performed to obtain *SMN2 $\Delta$ 7* homozygous transgenic animals, as determined by qPCR measurement of *SMN2 $\Delta$ 7* expression (Fig. 2 B).

Comparison of viability and body weight of the SMA $\Delta$ 7/*Sam68<sup>+/+</sup>* (*SMN2 $\Delta$ 7;SMN2;Snn<sup>-/-</sup>;Sam68<sup>+/+</sup>*) and SMA $\Delta$ 7/*Sam68<sup>-/-</sup>* (*SMN2 $\Delta$ 7;SMN2;Snn<sup>-/-</sup>;Sam68<sup>-/-</sup>*) mice revealed that ablation of SAM68 function affected the phenotype of SMA mice (Fig. 2 C). SMA $\Delta$ 7/*Sam68<sup>+/+</sup>* mice displayed a maximum survival of 14 d (mean survival = 11 d), whereas SMA $\Delta$ 7/*Sam68<sup>-/-</sup>* displayed a maximum survival of 20 d (mean survival = 16 d; Fig. 2 D). Thus, inhibition of SAM68 function in vivo significantly extended the life span of SMA $\Delta$ 7 mice.

The first phenotypic difference between SMA $\Delta$ 7/*Sam68<sup>+/+</sup>* and SMA $\Delta$ 7/*Sam68<sup>-/-</sup>* mice was body size (Fig. 2, C and E). The reduced weight of SMA $\Delta$ 7 mice was first appreciated at 5 d postpartum (dpp; Le et al., 2005). We found that the weight of SMA $\Delta$ 7/*Sam68<sup>+/+</sup>* did not increase significantly from 5 dpp to death; in contrast, SMA $\Delta$ 7/*Sam68<sup>-/-</sup>* mice steadily increased in size until 11 dpp, after which body weight started to decline (Fig. 2 E). Importantly, *Sam68<sup>-/-</sup>* mice are smaller than wild-type littermates (Fig. 2, C and E), indicating that this phenotype might partially limit the recovery in body weight observed in the SMA $\Delta$ 7 context.

Next, we measured the motor function of the experimental mice. SMA $\Delta$ 7/*Sam68<sup>-/-</sup>* mice at 8 and 10 dpp displayed less difficulty than SMA $\Delta$ 7/*Sam68<sup>+/+</sup>* littermates in righting when placed on their sides (Fig. 2 F). At 8 dpp, 11 out of 12 SMA $\Delta$ 7/*Sam68<sup>-/-</sup>* mice were able to right themselves, whereas 60% of the SMA $\Delta$ 7/*Sam68<sup>+/+</sup>* ( $n = 10$ ) could not, and the rest were slower (Fig. 2 F). The difference was maintained at 10 dpp, when five out of six SMA $\Delta$ 7/*Sam68<sup>-/-</sup>* mice were able to right themselves in the time frame of the test, whereas none of the SMA $\Delta$ 7/*Sam68<sup>+/+</sup>* mice did (Fig. 2 F). Non-SMA *Sam68<sup>-/-</sup>* mice could readily right themselves at these ages (Fig. S1 B).

These results suggest that deletion of SAM68 function partially rescues postnatal development and the life span of SMA $\Delta$ 7 mice.

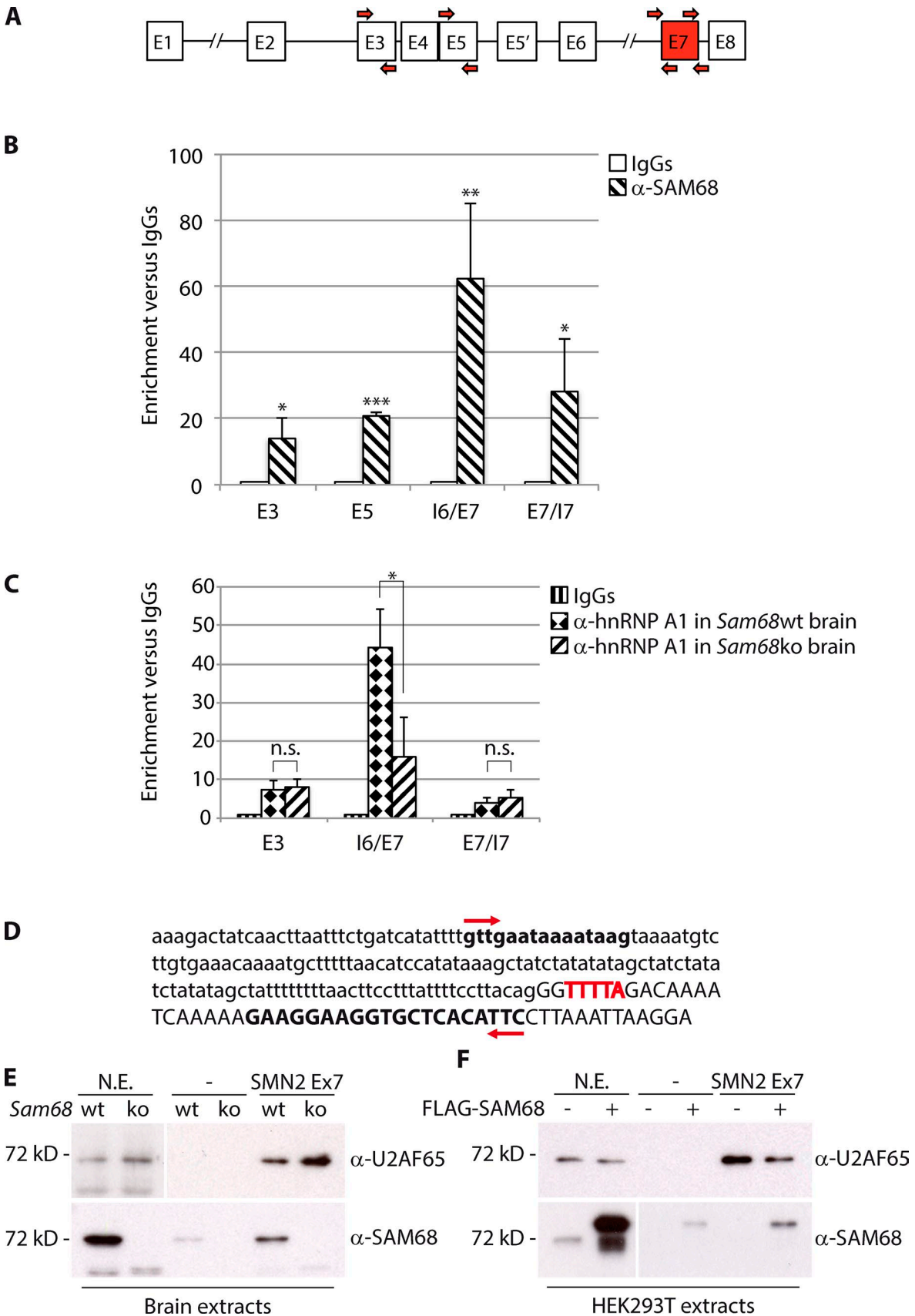


Figure 1. **SAM68 binds SMN2 exon 7 and mediates recruitment of hnRNP A1 in vivo.** (A) Schematic representation of the human SMN2 gene. Boxes represent exons, black lines represent introns, and the red box indicates the regulated exon 7. Red arrows indicate the oligonucleotide pairs used in the analysis. (B) CLIP assay of SAM68-bound SMN2 pre-mRNA in brain of non-SMA mice (*SMN2 $\Delta$ 7;SMN2;Snn<sup>+/+</sup>*). (C) CLIP assay of hnRNP A1 in brain

### **Sam68 deletion rescues SMN2 splicing and expression in SMAΔ7 tissues**

We then tested whether the partial rescue of the phenotype observed in SMAΔ7/*Sam68*<sup>-/-</sup> mice correlated with improvement of *SMN2* splicing and expression. To this end, cortex, cerebellum, spinal cord, liver, heart, kidney, and lung samples from 10-dpp SMAΔ7/*Sam68*<sup>+/+</sup> and SMAΔ7/*Sam68*<sup>-/-</sup> mice were collected for qPCR and Western blot analyses. Remarkably, *Sam68* ablation resulted in an increase of exon 7 inclusion in all tissues analyzed (Fig. 3 A). Normalization of *SMN2* exon 6 expression with Actin mRNA showed that there was no general increase in *SMN2* transcription (Fig. S2 A), ruling out increased transcription or stability as part of the mechanism. Improved *SMN2* exon 7 splicing correlated with an increase in SMN protein expression in SMAΔ7/*Sam68*<sup>-/-</sup> mice with respect to SMAΔ7/*Sam68*<sup>+/+</sup> littermates, particularly in cortex and cerebellum (Fig. 3 B; and Fig. S2, B and C). Expression of GEMIN2, which is degraded when the SMN complex is less abundant and/or functionally impaired (Feng et al., 2005), was also significantly increased in cortex and cerebellum of SMAΔ7/*Sam68*<sup>-/-</sup> with respect to those of SMAΔ7/*Sam68*<sup>+/+</sup> mice (Fig. S2, B and C). Conversely, ablation of *Sam68* in a non-SMA context, where the *SMN1*-like murine *Smn* gene contributes to the large majority of SMN protein expression, did not exert any effect (Fig. S2 D), indicating that SAM68 specifically functions on the human *SMN2* transgene.

### **Ablation of Sam68 rescues SMN assembly into nuclear gems in spinal cord motor neurons**

The SMA phenotype is mainly caused by degeneration of motor neurons in the spinal cord as a consequence of low SMN expression (Arnold and Burghes, 2013; Nurputra et al., 2013). Notably, we found that SAM68 is expressed at much higher levels in motor neurons than in the surrounding cells of the spinal cord (Fig. 4 A). Thus, we set out to investigate whether loss of SAM68 function affected the expression of SMN in motor neurons. Because SMN levels and functionality correlate with its accumulation in nuclear structures named gems (Li et al., 2014), we tested whether SAM68 expression affected its subcellular localization. Spinal cords from 8-dpp non-SMA, SMAΔ7/*Sam68*<sup>+/+</sup>, and SMAΔ7/*Sam68*<sup>-/-</sup> mice were collected and stained for SMN and for the motor neuron marker choline acetyltransferase (ChAT). As expected (Branchu et al., 2013), SMN gems were almost absent in most motor neurons of SMAΔ7 mice (Fig. 4, B and C). However, knockout of *Sam68* significantly increased the number of gems per motor neuron and the percentage of gem-containing motor neurons (Fig. 4, B and C), indicating that the increase in SMN protein expression was functionally relevant in the spinal cord.

### **Ablation of Sam68 rescues motor neuron loss in the spinal cord of SMAΔ7 mice**

Progressive degeneration of motor neurons in the ventral horns of the spinal cord is the main hallmark of SMA (Arnold and Burghes, 2013; Nurputra et al., 2013). To test whether inhibition of SAM68 function affected the number of motor neurons in SMAΔ7 mice, coronal sections of the lumbar spinal cord (L1–L5) were stained with Nissl substance (Fig. 5, A and B). An unbiased count of the total number of motor neurons (see Materials and methods section Motor neuron count in lumbar spinal cord) indicated that SMAΔ7 mice displayed >50% reduction in the number of motor neurons at 8 dpp with respect to non-SMA mice (Fig. 5, B and C). In line with the recovery in SMN expression and nuclear gems assembly, ablation of *Sam68* significantly promoted maintenance of motor neurons (Fig. 5, B and C), confirming that the rescue of SMN expression in these cells was functionally relevant.

### **Innervation of NMJs is ameliorated in SMAΔ7/Sam68<sup>-/-</sup> mice**

Several axial and appendicular muscles of SMAΔ7 mice display denervation of NMJs (Ling et al., 2012). Thus, we tested whether *Sam68* expression affected the proper innervation of NMJs in muscles of 10-dpp non-SMA and SMAΔ7 mice. Motor endplates were identified by confocal analyses with fluorophore-conjugated α-bungarotoxin, which specifically stains the subunit of acetylcholine receptors (AChRs), and nerve terminals were stained with antisynaptophysin and with an antibody directed against neurofilament heavy chains (Le et al., 2005; Hua et al., 2011). Analysis of the flexor digitorum brevis 2 (FDB2), one of the most vulnerable appendicular muscles in SMAΔ7 mice (Ling et al., 2012), showed a twofold increase in denervated NMJs in SMAΔ7/*Sam68*<sup>+/+</sup> mice compared with age-matched non-SMA mice (Fig. 6, A and B). Importantly, this defect was rescued in the SMAΔ7/*Sam68*<sup>-/-</sup> mice (Fig. 6, A and B). No significant difference in NMJ innervation was observed in FDB2 muscles from non-SMA mice that were either wild type or knockout for *Sam68* (Fig. 6 B). The rescue of innervation in SMAΔ7/*Sam68*<sup>-/-</sup> mice was also observed in the masseter (Fig. S3, A and B), one of the most vulnerable axial muscles in SMAΔ7 mice (Ling et al., 2012). These results indicate that *Sam68* depletion improves innervation of NMJs in a mouse model of SMA.

### **Skeletal muscle atrophy and peripheral organ phenotypes are improved in SMAΔ7/Sam68<sup>-/-</sup> mice**

NMJ denervation in SMAΔ7 mice leads to skeletal muscle atrophy without showing dystrophic features (Le et al., 2005). Consistently, as shown by the frequency distribution of the cross-sectional area (CSA), myofibers from triceps of 10-dpp SMAΔ7/*Sam68*<sup>+/+</sup> mice were significantly smaller than those

---

of non-SMA mice that are wild type or knockout for *Sam68*. Signals for SAM68 (B) and hnRNP A1 (C) binding was calculated as fold enrichment versus IgGs and expressed as mean ± SD; n = 3. The p-value was determined by two-tailed *t* test (B) or one-way ANOVA test followed by Bonferroni's multiple comparison posttest (C). \*, P < 0.05; \*\*, P ≤ 0.01; \*\*\*, P ≤ 0.001; n.s., not significant (P > 0.05). (D) Sequence of human *SMN2* probe used to synthesize the biotinylated RNA for the streptavidin pull-down experiment. Lowercase letters indicate the intron 6 sequence; uppercase letters indicate the exon 7 sequence. Bold letters and red arrows indicate primers used to synthesize the probe, and red bold letters indicate the exonic splicing silencers created by the C to T transition in *SMN2* to which SAM68 binds. [E and F] Western blot analysis of the binding of endogenous U2AF65 to the biotinylated probe (*SMN2* Ex7) in streptavidin pull-down assays using brain extracts from non-SMA *Sam68*<sup>+/+</sup> (wt) or *Sam68*<sup>-/-</sup> (ko) mice (E) or extracts from HEK293T cells transfected (+) or not (-) with FLAG-SAM68 (F). Results are representative of three experiments that yielded similar results. ko, knockout; N.E., nuclear extracts; wt, wild type.

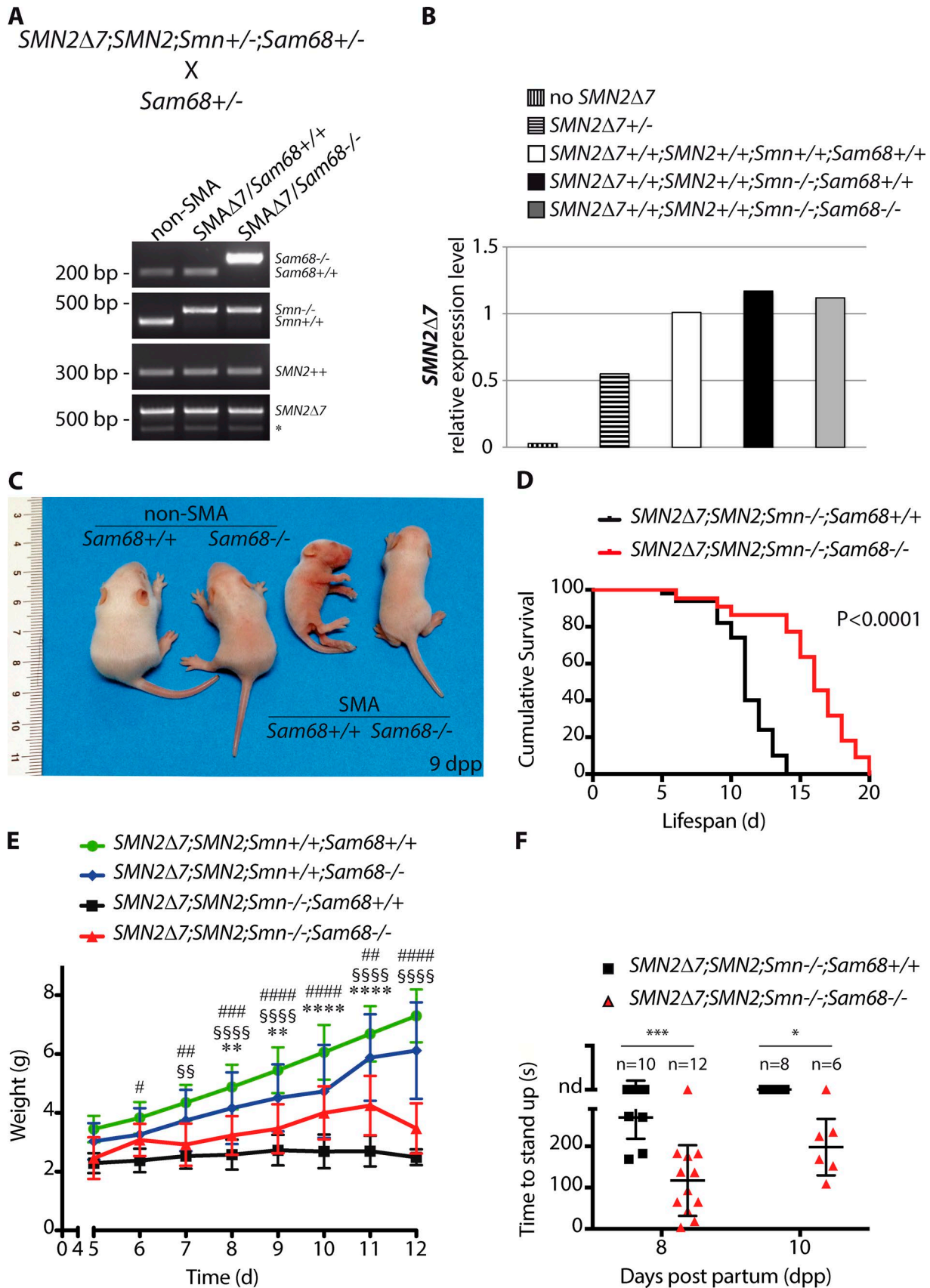


Figure 2. **Ablation of *Sam68* expression partially rescues viability, body weight, and motor function of *SMAΔ7* mice.** (A) Schematic diagram of transgenic mice crossing (top) and PCR analysis of genomic DNA (bottom) from tails of  $SMN2\Delta7;SMN2;Smn^{+/-};Sam68^{+/+}$  (first lane),  $SMN2\Delta7;SMN2;Smn^{-/-};Sam68^{+/+}$  (second lane), and  $SMN2\Delta7;SMN2;Smn^{-/-};Sam68^{-/-}$  (third lane) mice. Bands showing the transgenic and endogenous DNA bands amplified are indi-

of non-SMA littermates (Fig. 7, A and B). Notably, muscles of SMA $\Delta 7/Sam68^{-/-}$  mice were characterized by bigger myofibers than those of SMA $\Delta 7/Sam68^{+/+}$  littermates (Fig. 7, A and B), with the frequency distribution of CSA revealing a significant shift of the median value toward the larger size of fibers (Fig. 7 B). In non-SMA mice, knockout of *Sam68* did not affect the size of myofibers (Fig. 7 B).

Skeletal muscle atrophy in SMA mice is accompanied by elevated expression of atrophy-related genes (Bricceno et al., 2012). The transcription factors FoxO3 and NF- $\kappa$ B are involved in activation of the ubiquitin–proteasome system and autophagy (Cai et al., 2004; Mammucari et al., 2007), two important intracellular degradation mechanisms responsible for skeletal muscle atrophy. Thus, we analyzed targets of FoxO3 and NF- $\kappa$ B (Cai et al., 2004; Mammucari et al., 2007), such as *Trim63/MuRF1*, *Atrogin1/MAFbx*, and *Cathepsin L*, in SMA $\Delta 7/Sam68^{+/+}$  and SMA $\Delta 7/Sam68^{-/-}$  mice. *Trim63*, *Atrogin1*, and *Cathepsin L* were significantly up-regulated in muscles of SMA $\Delta 7/Sam68^{+/+}$  mice; however, their expression was reduced to the levels of control mice in muscles from SMA $\Delta 7/Sam68^{-/-}$  mice (Fig. 7 C). Expression of these genes was not affected in non-SMA *Sam68^{-/-}* mice (Fig. 7 C). These findings indicate that ablation of *Sam68* rescues skeletal muscle atrophy in SMA $\Delta 7$  mice.

SMA mouse models also display defects in peripheral organs, such as the liver (Hua et al., 2011) and heart (Shababi et al., 2010). For instance, decreased expression of hepatic *insulin-like growth factor (IGF)–binding protein acid labile subunit (Igfals)* in neonatal SMA mice caused pronounced reduction of circulating IGF-1, which was suggested to contribute to the phenotype (Hua et al., 2011). Expression of *Igf-1* and *Igfals* was strongly reduced in the liver of 10-dpp SMA $\Delta 7/Sam68^{+/+}$  mice, whereas this defect was attenuated in SMA $\Delta 7/Sam68^{-/-}$  mice (Fig. S4 A). Moreover, histological examination showed hepatic steatosis accompanied by an influx of inflammatory cells in SMA $\Delta 7/Sam68^{+/+}$  mice, but not in the liver of SMA $\Delta 7/Sam68^{-/-}$  mice, which resembled that of control mice (Fig. S4 B).

SMA mice show signs of oxidative stress in the heart, such as elevated expression of *Angiotensin 1 receptor (AT1R)*, *Rac1*, and *Nox2* (Shababi et al., 2010). Expression of *AT1R* and *Rac1* was increased in the liver (Fig. S4 C) and heart (Fig. S4 D) of SMA $\Delta 7/Sam68^{+/+}$  mice, whereas *Nox2* was up-regulated only in the heart (Fig. S4 D). SMA $\Delta 7/Sam68^{-/-}$  mice showed lower expression levels of *AT1R* and *Rac1* in these organs (Fig. S4, C and D), resembling those of non-SMA mice. None of these parameters in peripheral organs were affected in non-SMA *Sam68^{-/-}* mice (Fig. S4, A, C, and D; and unpublished data).

The thickness of the interventricular septum (IVS) is reduced in SMA mice (Shababi et al., 2010; Hua et al., 2011). Accordingly, SMA $\Delta 7/Sam68^{+/+}$  mice showed an ~60% re-

duction in IVS thickness compared with the non-SMA littermates, whereas this reduction was partially compensated for in SMA $\Delta 7/Sam68^{-/-}$  mice (Fig. S4 E). Collectively, these results indicate that ablation of *Sam68* also improves defects in the peripheral organs of SMA $\Delta 7$  mice.

## Discussion

Our work identifies SAM68 as a physiological regulator of *SMN2* splicing. SAM68 binds *SMN2* pre-mRNA *in vivo* near the 3' ss of exon 7 and favors recruitment of hnRNP A1, while interfering with that of U2AF. Thus, our results suggest that SAM68 forms a repressive complex masking the 3' ss and prevents its recognition by the spliceosome, causing exon 7 skipping and expression of the unstable *SMN $\Delta 7$*  variant. Importantly, ablation of *Sam68* expression partially rescues *SMN2* splicing and expression, resulting in increased viability and amelioration of the phenotype of SMA $\Delta 7$  mice.

SMA is caused by the inability of the *SMN2* gene to compensate for the functional loss of *SMN1* in patients (Arnold and Burghes, 2013; Nurputra et al., 2013). Because exon 7 skipping is the major cause of the decreased function of *SMN2*, characterization of the splicing factors and molecular mechanisms regulating this splicing event is of crucial relevance for understanding the cause of SMA and for the design of therapeutic approaches (Lorson and Lorson, 2012). An advance in this direction was provided by the identification of RBPs capable of modulating *SMN2* splicing in cultured cells (Hofmann et al., 2000; Hofmann and Wirth, 2002; Kashima and Manley, 2003; Kashima et al., 2007; Bose et al., 2008; Chen et al., 2008; Pedrotti et al., 2010; Singh et al., 2011). However, whether any of these splicing regulators contribute to the phenotype of SMA is still currently unknown, as a role in the onset or progression of SMA has not been demonstrated for any of them. This is particularly relevant because splicing is a tissue- and cell context-specific combinatorial process (Fu and Ares, 2014). For instance, TRA2- $\beta$  is a strong inducer of exon 7 inclusion in cultured cells (Hofmann et al., 2000), but its conditional knockout showed no effect on *SMN2* splicing in motor neurons (Mende et al., 2010). These findings highlight the complexity of alternative splicing regulation *in vivo* and call for mechanistic studies to be performed directly in the cells or tissues that are relevant for the disease.

Our work was aimed at elucidating whether SAM68 is a physiological regulator of *SMN2* splicing using an SMA mouse model. The SMA $\Delta 7$  mice used in our study display a severe form of the disease and die within 2 wk of birth (Le et al., 2005). Knockout of *Sam68* expression in this strain resulted in significant body weight gain and extended survival until 20 dpp.

cated; the asterisk indicates an undefined band present in SMA $\Delta 7$  transgenic mice. (B) qPCR of *SMN2 $\Delta 7$*  to quantify the dosage of transgenic *SMN2 $\Delta 7$*  in hemizygous and homozygous transgenic animals. The data shown are from a single representative experiment, and values were normalized with Apolipoprotein B mRNA. (C) Micrograph showing representative non-SMA and SMA $\Delta 7$  (SMA) mice that are either wild type (*Sam68^{+/+}*) or knockout (*Sam68^{-/-}*) for *Sam68*. (D) Kaplan-Meier survival curves of SMA $\Delta 7/Sam68^{+/+}$  ( $n = 50$ ) and SMA $\Delta 7/Sam68^{-/-}$  ( $n = 22$ ). Statistical analysis was performed by the log-rank test ( $P < 0.0001$ ). (E) Weight curves of non-SMA/*Sam68^{+/+}*, non-SMA/*Sam68^{-/-}*, SMA $\Delta 7/Sam68^{+/+}$ , and SMA $\Delta 7/Sam68^{-/-}$  mice. Plot shows mean  $\pm$  SD of at least 15 mice for each group for each day analyzed. The p-values were determined by a two-way ANOVA test followed by Bonferroni's multiple comparison posttest. # represents the p-value of the non-SMA/*Sam68^{+/+}* versus non-SMA/*Sam68^{-/-}* comparison; § represents the p-value of the non-SMA/*Sam68^{-/-}* versus SMA $\Delta 7/Sam68^{-/-}$  comparison; and \* represents the p-value of the SMA $\Delta 7/Sam68^{+/+}$  versus SMA $\Delta 7/Sam68^{-/-}$  comparison. For all comparisons,  $P < 0.05$ ,  $P < 0.01$ ,  $P < 0.001$ , and  $P < 0.0001$  are represented by increasing symbols (from one to four). (F) Time required for pups to stand up after being placed on their sides for SMA $\Delta 7/Sam68^{+/+}$  mice compared with SMA $\Delta 7/Sam68^{-/-}$  mice at 8 and 10 dpp (nd [nondetected] indicates experimental animals that never stood up during the test). Statistical analysis was performed by two-way ANOVA test followed by Bonferroni's multiple comparison posttest (\*,  $P < 0.05$ ; \*\*\*,  $P < 0.001$ ).

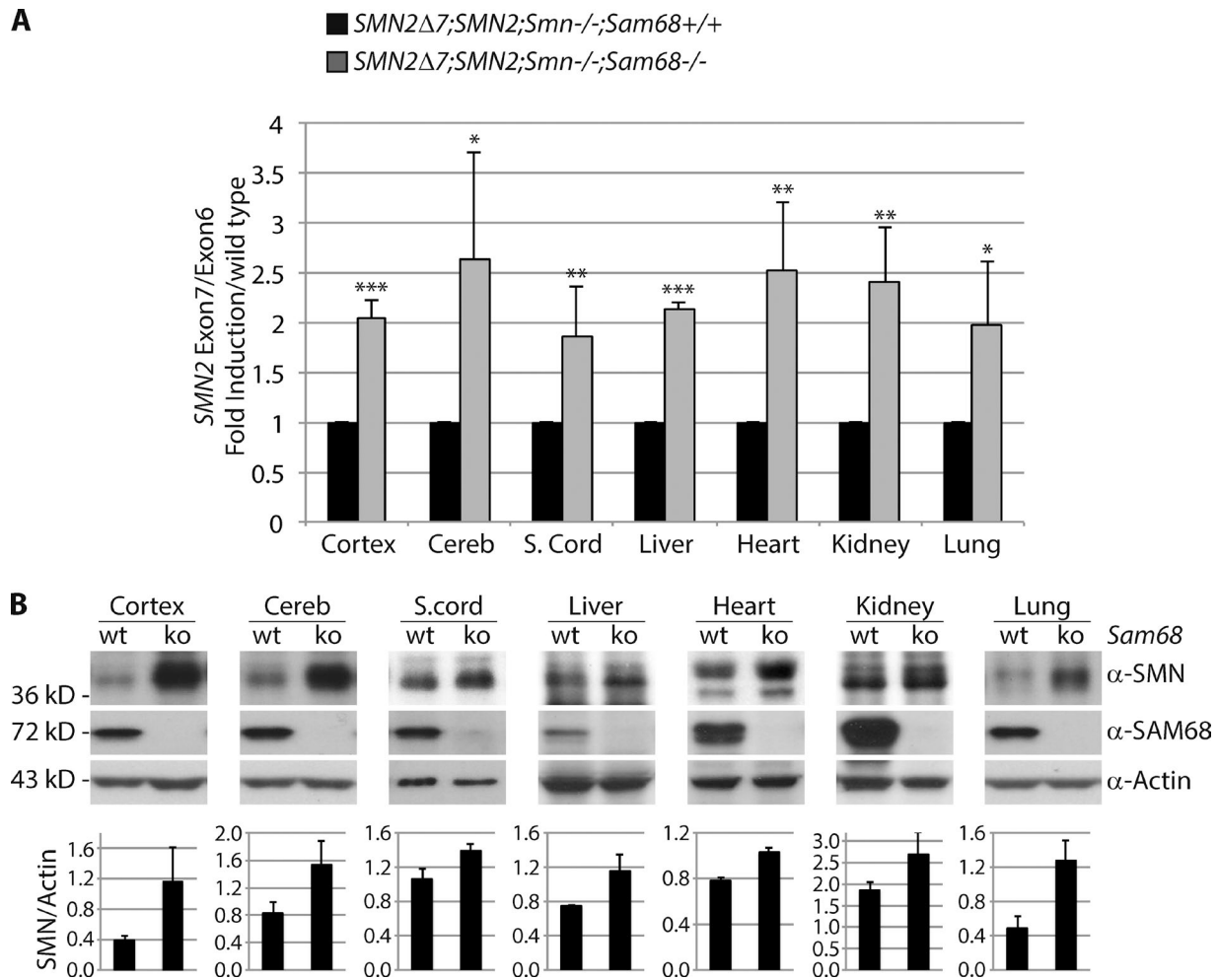


Figure 3. ***Sam68* deletion rescues *SMN2* splicing and expression in *SMA $\Delta$ 7* tissues.** (A) qPCR analysis of exon 7-containing *SMN2* transgene transcripts normalized to constant exon 6 in tissues of 10-dpp *SMA $\Delta$ 7/Sam68<sup>+/+</sup>* and *SMA $\Delta$ 7/Sam68<sup>-/-</sup>* mice. Bar graph represents mean  $\pm$  SD.  $n = 3$ . The p-value was determined by two-tailed  $t$  test (\*,  $P \leq 0.05$ ; \*\*,  $P \leq 0.01$ ; \*\*\*,  $P \leq 0.001$ ). (B) Western blot analysis of SMN protein expression in the indicated tissues of 10-dpp *SMA $\Delta$ 7/Sam68<sup>+/+</sup>* (wt) or *SMA $\Delta$ 7/Sam68<sup>-/-</sup>* (ko) mice. Actin was used as a loading control. Quantification of the SMN band is shown at the bottom. Each point value represents the mean  $\pm$  SD.  $n = 2$ . Cereb, cerebellum; ko, knockout; S.cord, spinal cord; wt, wild type.

Several pieces of evidence suggest that the impact of SAM68 on the SMA phenotype directly relates to its ability to modulate *SMN2* splicing in vivo. First, SAM68 is recruited near the 3' ss of exon 7 in the brain of mice expressing the human *SMN2* transgene (Fig. 1 B). Furthermore, observations gathered using cell culture systems indicate that SAM68 interacts and cooperates with hnRNP A1 (Paronetto et al., 2007; Pedrotti et al., 2010), one of the best-characterized repressors of *SMN2* exon 7 inclusion (Kashima and Manley, 2003; Kashima et al., 2007). Our findings now indicate that this cooperation is relevant in the context of SMA in vivo. Binding of hnRNP A1 in proximity to the 3' ss of exon 7 was strongly reduced in the absence of SAM68 (Fig. 1 C). In contrast, we found an inverse correlation between binding of SAM68 and U2AF65 to exon 7 in vitro, with increased recruitment of this general splicing factor in brain extracts of *Sam68<sup>-/-</sup>* mice (Fig. 1 E). Thus, we propose a model in which SAM68 binds to the *SMN2* pre-mRNA near the 3' ss of exon 7, favoring the recruitment of hnRNP A1. Formation of this inhibitory complex on the nascent pre-mRNA interferes with binding of U2AF and efficient recognition of the 3' ss, thereby masking the exon and favoring its skipping from the mature mRNA.

Regulation of *SMN2* splicing by SAM68 is likely to affect the SMA phenotype directly. We found that ablation of *Sam68* expression increased *SMN2* exon 7 inclusion in the central nervous system and in all peripheral tissues analyzed (Fig. 3 A). Furthermore, enhanced exon 7 splicing resulted in higher SMN expression (Fig. 3 B). SMN is a ubiquitous protein that localizes to both the cytoplasm and nucleus, where it accumulates in nuclear gems that are implicated in RNP assembly and maturation (Li et al., 2014). SMN gems were increased in motor neurons of the *SMA $\Delta$ 7/Sam68<sup>-/-</sup>* spinal cord (Fig. 4, B and C), thus providing a robust readout for functional SMN. Moreover, ablation of *Sam68* partially rescued the loss of motor neurons occurring in the spinal cord of *SMA $\Delta$ 7* mice (Fig. 5). Notably, SAM68 expression is much higher in motor neurons than in surrounding cells of the spinal cord (Fig. 4 A), which may explain the particularly inefficient inclusion of exon 7 observed in motor neurons (Ruggiu et al., 2012). Collectively, these findings suggest that SAM68 physiologically participates in regulation of the disease-related *SMN2* splicing and that amelioration of the SMA phenotype is likely a result of splicing-dependent stabilization of SMN protein in the absence of SAM68. However, the beneficial effect of *Sam68* ablation on the splicing of *SMN2* could be

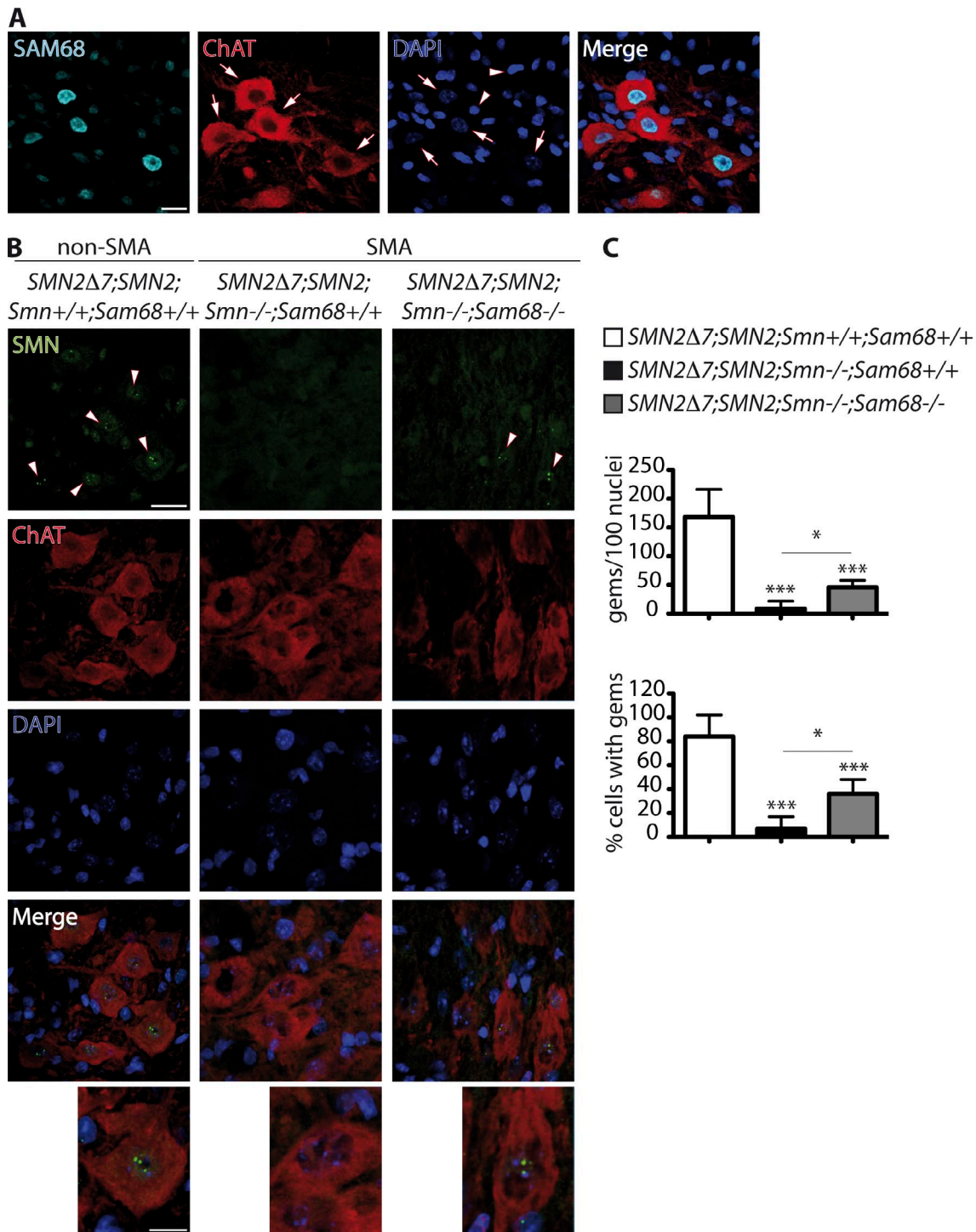
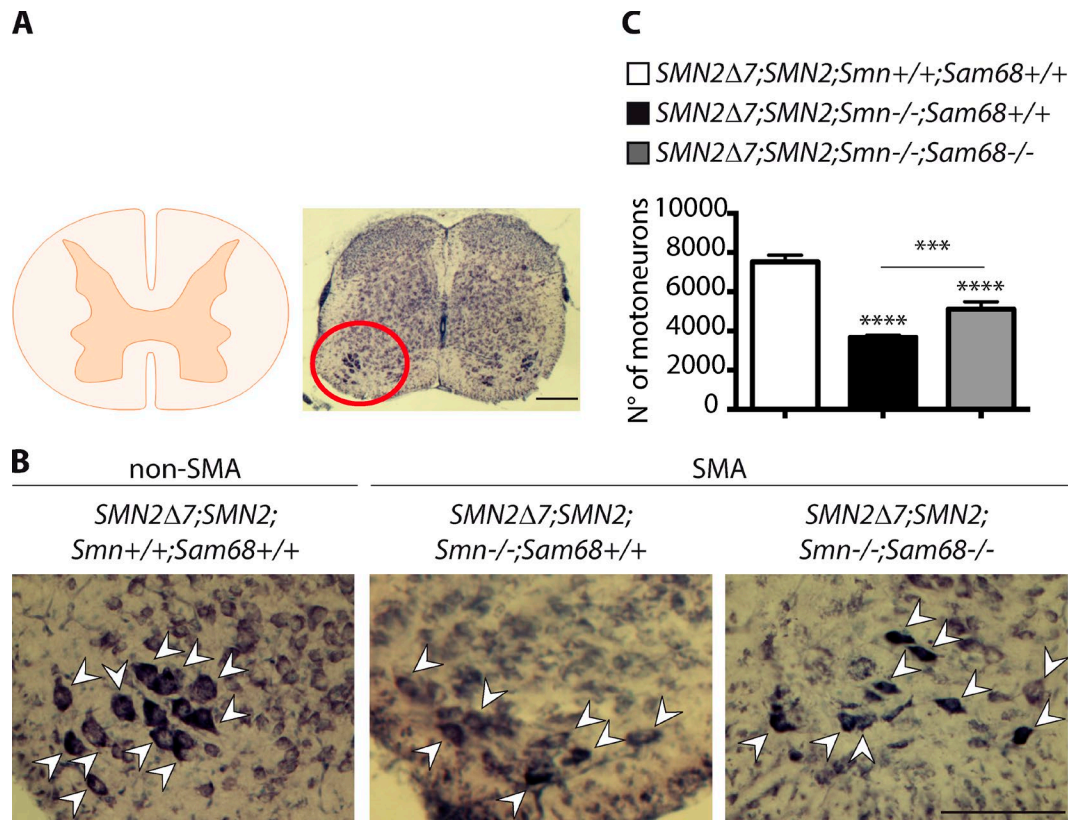


Figure 4. **Ablation of *Sam68* rescues SMN assembly into nuclear gems in spinal cord motor neurons.** (A) Immunodetection of SAM68 (blue) in ChAT-positive motor neurons (red) in the lumbar spinal cord (L1–L5) of 8-dpp non-SMA mice. DAPI was used for staining of nuclei. Motor neurons are indicated by arrows and surrounding cells by arrowheads. (B) Immunodetection of SMN gems (green) in ChAT-positive motor neurons (red) in the spinal cord (L1–L5) of 8-dpp non-SMA, *SMAΔ7/Sam68<sup>+/+</sup>*, and *SMAΔ7/Sam68<sup>-/-</sup>* (SMA) mice. DAPI was used for staining of nuclei. Nuclear gems are indicated by arrowheads. Bars: (A and B) 20 μm; (insets) 10 μm. (C) Quantitative analysis of SMN gems in spinal motor neurons. The bar graph (mean ± SD; *n* = 3) shows the number of gems per 100 nuclei analyzed per sample (top) and the percentage of gem-positive motor neurons (bottom). Statistical analysis was performed by one-way ANOVA test followed by Bonferroni's multiple comparison posttest (\*, *P* < 0.05; \*\*\*, *P* < 0.001).

partially limited by the presence of SLM2, a homologous protein expressed in the brain (Ehrmann et al., 2013). SLM2 could partially complement the SAM68 splicing-repressive activity in *Sam68<sup>-/-</sup>* mice, as the two proteins bind almost identical RNA

sequences (Galarneau and Richard, 2009). Moreover, we found that SLM2 also binds to the SMN2 pre-mRNA in vivo and can promote exon 7 skipping in transfected cells (unpublished data). Thus, as also suggested by the residual CLIP signal in





**Figure 5. Ablation of *Sam68* rescues motor neuron loss in the spinal cord of SMA $\Delta$ 7 mice.** (A) Schematic representation of a Nissl-stained spinal cord section of the lumbar spinal cord from 8-dpp non-SMA mice (right). The red circle highlights the ventral horn of the spinal cord analyzed. Bar, 250  $\mu$ m. (B) Higher magnification of sections of the ventral lumbar spinal cord from 8-dpp non-SMA, SMA $\Delta$ 7/*Sam68*<sup>+/+</sup>, and SMA $\Delta$ 7/*Sam68*<sup>-/-</sup> (SMA) mice. Motor neurons are indicated by arrowheads. Bar, 125  $\mu$ m. (C) Bar graph representing motor neuron counts (mean  $\pm$  SD;  $n = 3$ ) in lumbar spinal cord from mice described in B. Statistical analysis was performed by one-way ANOVA test followed by Bonferroni's multiple comparison posttest (\*\*\*,  $P < 0.001$ ; \*\*\*\*,  $P < 0.0001$ ).

*Sam68*<sup>-/-</sup> mice (Fig. S1 A), SLM2 might partially compensate for SAM68-dependent regulation of *SMN2* splicing.

Knockout of *Sam68* ameliorated hallmarks of the disease in SMA $\Delta$ 7 mice. In addition to the rescue in *SMN* expression and in the number of motor neurons, SMA $\Delta$ 7/*Sam68*<sup>-/-</sup> mice displayed an improvement in NMJ innervation and reduced muscle atrophy. Furthermore, ablation of *Sam68* also affected other phenotypes described in SMA mouse models. In particular, SMA $\Delta$ 7/*Sam68*<sup>-/-</sup> mice showed increased expression of IGF-1 pathway-related genes (*Igf-1* and *Igfals*) in the liver, which was accompanied by a general improvement in the physiology of the organ (Fig. S4, A–C). Improved function of the IGF-1 pathway in the liver was also elicited by antisense oligonucleotide-mediated correction of *SMN2* splicing, and it was supposed to contribute to improvement of the SMA phenotype (Hua et al., 2011). Although defects in peripheral organs have not been confirmed in SMA patients (Iascone et al., 2015), our observations suggest that increased expression of *Igf-1* and *Igfals* and the general improvement of liver function in SMA $\Delta$ 7/*Sam68*<sup>-/-</sup> mice might contribute to amelioration of the SMA phenotype observed in this study.

Although ablation of *Sam68* expression caused a ubiquitous increase in *SMN* expression and ameliorated several hallmarks of SMA, we observed only a modest improvement in body weight and viability of SMA $\Delta$ 7/*Sam68*<sup>-/-</sup> mice. Regarding the limited increase in body weight, this is likely because of the smaller size of prepubertal non-SMA *Sam68*<sup>-/-</sup> mice (Fig. 2,

C and E), similar to what was reported for adult *Sam68*<sup>-/-</sup> mice (Richard et al., 2005; Paronetto et al., 2009). However, the limited effect on viability might result from other phenotypes described for this mouse. *Sam68*<sup>-/-</sup> mice have a relatively high perinatal lethality, with 30–35% of mice dying before weaning (Richard et al., 2005). Although the exact cause of decreased viability is still currently unknown, it is likely linked to the reported changes in target RNA expression and splicing in several organs (Paronetto et al., 2009; Bianchi et al., 2010; Huot et al., 2012), including the brain (Iijima et al., 2011). Thus, it is possible that other changes in gene expression and splicing caused by *Sam68* ablation elicit deleterious effects that attenuate the benefit of the increased expression of *SMN* on the phenotype of SMA $\Delta$ 7/*Sam68*<sup>-/-</sup> mice.

In conclusion, our work shows for the first time that direct interference with the endogenous expression of a single splicing factor rescues *SMN2* splicing and expression in an SMA mouse model, resulting in amelioration of the phenotype. Thus, these findings strongly support a direct role for SAM68 in the pathology of SMA.

## Materials and methods

### Generation of transgenic mice and breeding strategy

*Sam68*<sup>+/+</sup> mice were generated by replacing exon 4 and part of exon 5 with a neomycin-resistant gene cassette as previously characterized

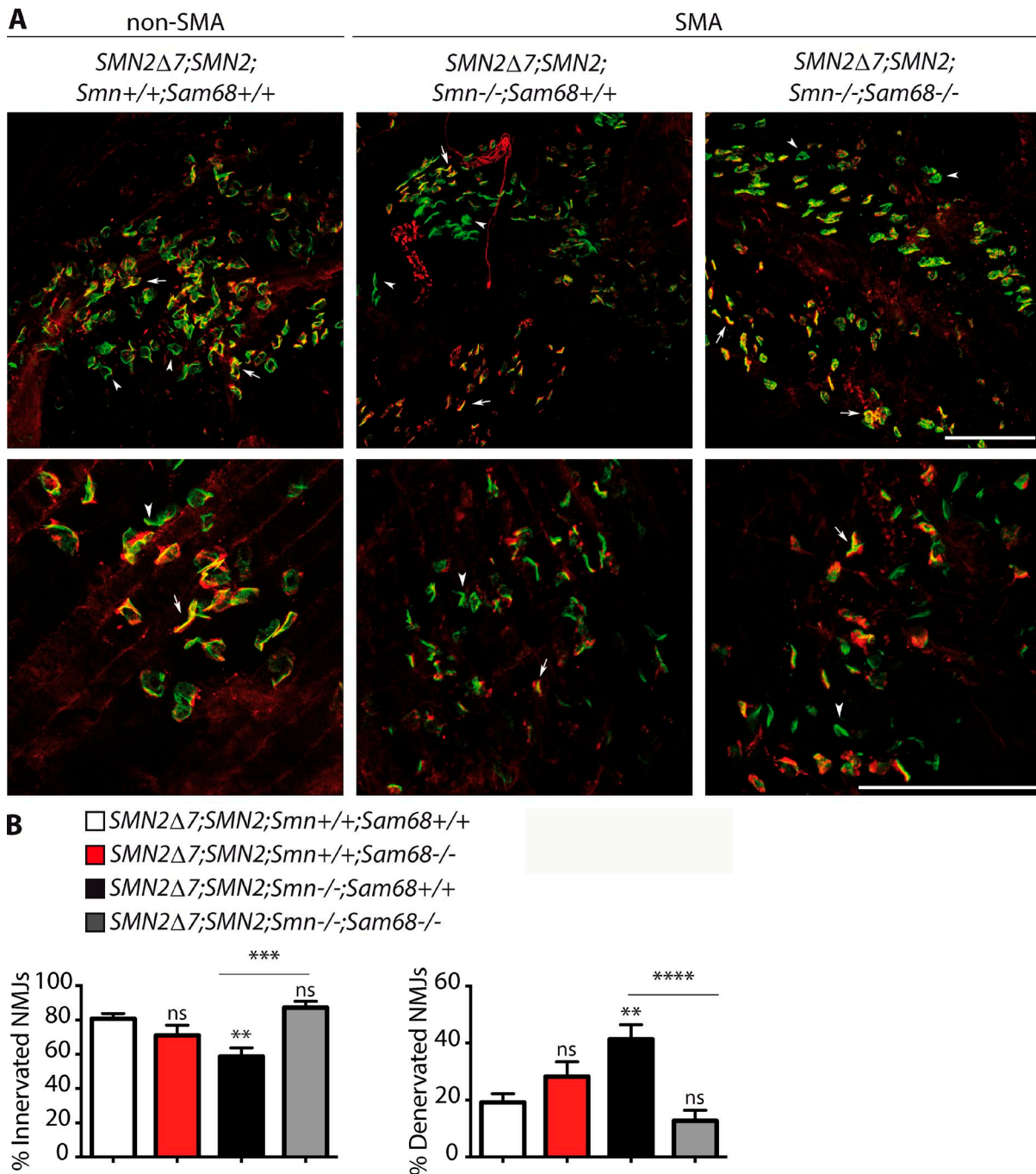


**Figure 6. Ablation of *Sam68* ameliorates innervation of NMJs.** (A) NMJ immunofluorescence images from whole-mount FDB2 of 10-dpp non-SMA, SMA $\Delta$ 7/*Sam68*<sup>+/+</sup>, and SMA $\Delta$ 7/*Sam68*<sup>-/-</sup> (SMA) mice. Higher magnifications are shown in the bottom panels. Postsynaptic (AChRs stained with  $\alpha$ -bungarotoxin; green), presynaptic (stained with  $\alpha$ -synaptophysin; red), and motor neuron axons (stained with an antibody against the heavy chain of neurofilament; red) were visualized. Bars, 100  $\mu$ m. Arrows point to innervated NMJs (yellow staining), and arrowheads point to denervated NMJs (green staining). (B) Bar graph showing the percentage of innervated (left) and denervated (right) NMJs in FDB2 of non-SMA, non-SMA/*Sam68*<sup>-/-</sup>, SMA $\Delta$ 7/*Sam68*<sup>+/+</sup>, and SMA $\Delta$ 7/*Sam68*<sup>-/-</sup> mice [for all,  $n = 3$ ]. Quantification of NMJ innervation was performed on at least 100 optical sections for mice, with a step size of 3  $\mu$ m from the whole FDB2 of each genotype. Data represent mean  $\pm$  SEM. Statistical analysis was performed by one-way ANOVA followed by Bonferroni's multiple comparison posttest (\*\*,  $P < 0.01$ ; \*\*\*,  $P < 0.001$ ; \*\*\*\*,  $P < 0.0001$ ; ns, not significant [ $P > 0.05$ ]).

(Richard et al., 2005). The SMA mouse model used was FVB. Cg-Tg(SMN2\*delta7)4299Ahmb Tg(SMN2)89Ahmb *Smn1tm1Msd/J* (The Jackson Laboratory), hereafter referred to as SMA $\Delta$ 7 mice. The SMA $\Delta$ 7 mouse model was provided by F. Sanguolo (University of Rome Tor Vergata, Rome, Italy). *SMN2 $\Delta$ 7;SMN2;Smn<sup>+/+</sup>* transgenic mice were crossed with *Sam68*<sup>+/+</sup> mice to obtain *SMN2 $\Delta$ 7;SMN2;Smn<sup>+/+</sup>;Sam68*<sup>+/+</sup> mice on an FVB/N  $\times$  C57BL/6 hybrid background. Mice were inter-

bred to obtain SMA $\Delta$ 7 mice (*SMN2 $\Delta$ 7;SMN2;Smn<sup>-/-</sup>*) that were wild type (*Sam68*<sup>+/+</sup>) or knockout (*Sam68*<sup>-/-</sup>) for *Sam68*. Breeding and maintenance of mice were done in accordance with the institutional guidelines of the University of Rome Tor Vergata and the approval of the Ethical Committee. Genomic DNA was isolated from the tail, amplified by PCR using the primers listed in Table S1, and genotyped as described previously (Le et al., 2005). Body weight and life span

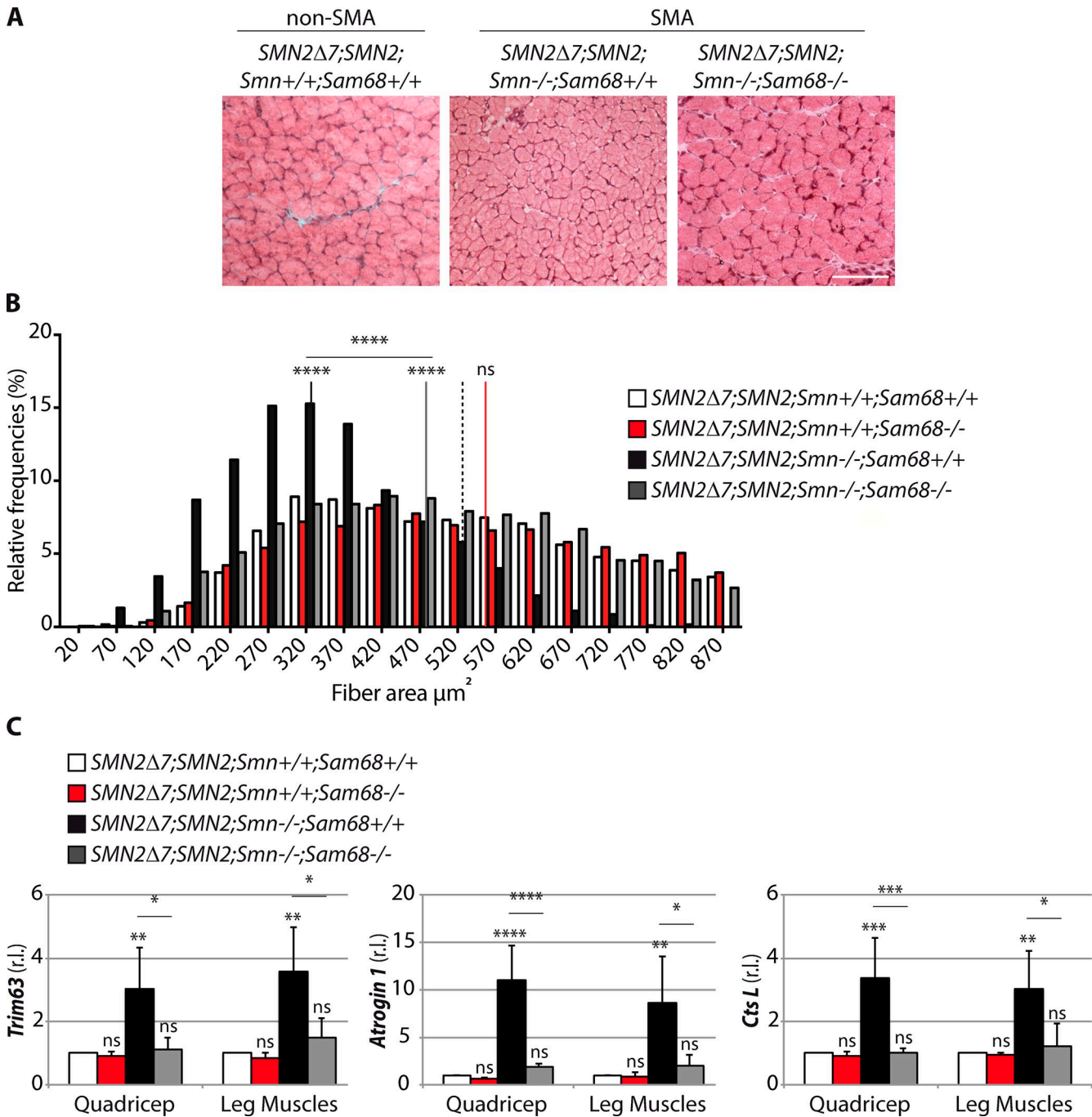


Figure 7. **Skeletal muscle atrophy is ameliorated in the SMA $\Delta$ 7/*Sam68*<sup>-/-</sup> mice.** (A) Hematoxylin and eosin staining of triceps muscle sections from 10-dpp non-SMA, SMA $\Delta$ 7/*Sam68*<sup>+/+</sup>, and SMA $\Delta$ 7/*Sam68*<sup>-/-</sup> (SMA) mice. Bar, 100  $\mu$ m. (B) Frequency distribution of muscle fiber areas (at least 2,000 for each genotype) of the experimental animals described in A. The colored lines and dotted line (non-SMA mice) represent the median value for each genotype: non-SMA mice ( $n = 3$ ) median size = 531  $\mu$ m<sup>2</sup> and fiber size (mean  $\pm$  SEM) = 568.76  $\pm$  5.8  $\mu$ m; non-SMA/*Sam68*<sup>-/-</sup> mice ( $n = 3$ ) median size = 557  $\mu$ m<sup>2</sup> and fiber size (mean  $\pm$  SEM) = 586.60  $\pm$  5.7  $\mu$ m; SMA $\Delta$ 7/*Sam68*<sup>+/+</sup> median size = 327  $\mu$ m<sup>2</sup> and fiber size (mean  $\pm$  SEM) = 342.32  $\pm$  3.1  $\mu$ m; and SMA $\Delta$ 7/*Sam68*<sup>-/-</sup> median size = 486  $\mu$ m<sup>2</sup> and fiber size (mean  $\pm$  SEM) = 503.59  $\pm$  4.6  $\mu$ m. Statistical analysis of the median values among groups was performed by one-way ANOVA test followed by Dunn's multiple comparison posttest. (C) qPCR analysis of the expression of atrophy-related genes in quadriceps and lower leg muscles of mice described in B. Values (mean  $\pm$  SD;  $n = 4$ ) were normalized with *Actin* mRNA. Statistical analysis was performed by one-way ANOVA test followed by Bonferroni's multiple comparison posttest. \*,  $P < 0.05$ ; \*\*,  $P < 0.01$ ; \*\*\*,  $P < 0.001$ ; \*\*\*\*,  $P < 0.0001$ ; ns, not significant ( $P > 0.05$ ). r.l., relative level.

recordings were performed every day until the natural death of the animal. The righting test (recorded at 8 and 10 dpp) measured the time taken by mice to get back on their feet after being placed on the right side. Each mouse was subjected to five successive attempts separated by a 5-min rest period.

#### Motor neuron count in lumbar spinal cord

Anesthetized animals were submitted to intracardial perfusion with PBS followed by 4% PFA diluted in PBS. Coronal sections of the lumbar spinal cord (L1–L5) were cut with a cryostat at 30- $\mu$ m thickness, and every seventh section was stained with Nissl substance. An op-

tical fractionator stereological design (West et al., 1991) was used to obtain unbiased estimates of the total number of motor neurons using the Stereo Investigator system (Stereo Investigator software, version 4.04; MicroBrightField). A stack of MAC 5000 controller modules (Ludl Electronic Products) was configured to interface with a microscope (BX 50; Olympus) with a motorized stage and a color digital camera (HV-C20; Hitachi) with a Pentium II PC workstation. A 3D optical dissector counting probe (x, y, and z dimensions of 30 × 30 × 10 μm, respectively) was applied to a systematic random sample of motor neurons in the lumbar spinal cord. The region of interest was outlined using the 10× objective, whereas the 100× oil immersion objective was used for marking individual motor neurons. The total motor neuron number was estimated according to the formula given below:

$$N = \sum Q \times \frac{1}{ssf} \times \frac{1}{asf} \times \frac{1}{tsf}.$$

$\sum Q$ , total number of motor neurons counted in all optical field samples of the lumbar spinal cord; *ssf*, section sampling fraction; *asf*, area sampling fraction; and *tsf*, thickness sampling fraction (defined by dissector height divided by estimated mean section thickness; Biamonte et al., 2009).

### Histology and immunofluorescence

Hearts were embedded in tissue-freezing medium, snap frozen in nitrogen-cooled isopentane, and stained. Transversal sections of 7 μm were arbitrarily chosen and photomicrographed using AxioVision 3.1 software (Carl Zeiss). IVS measurement was analyzed with ImageJ software (v.1.42q; National Institutes of Health) as described previously (Shababi et al., 2010).

For NMJ analysis, the FDB2 and masseter muscles were dissected and fixed in 4% PFA at 4°C for 180 min. Whole-mount muscles were immunostained with mouse antineurofilament (1:200; SMI-32; BioLegend) and rabbit antisynaptophysin (1:200; Thermo Fisher Scientific). Neurofilaments were visualized with TRITC AP donkey anti-mouse IgG (1:200; Jackson ImmunoResearch Laboratories, Inc.), and synaptic vesicles were visualized with Cy5 AP donkey anti-rabbit IgG (1:400; Jackson ImmunoResearch Laboratories, Inc.) secondary antibody. AChRs were labeled with Alexa Fluor 488-conjugated α-bungarotoxin (10 nM; Molecular Probes). Z-stack images were obtained at sequential focal planes 3 μm apart using a confocal microscope (Laser Scanning TCS SP2; Leica). Illustrated images are flattened projections of Z-stack images. Muscle innervation was analyzed with LAS AF Lite software (100 optical sections/genotype; Leica), and the innervation status of individual postsynaptic endplates was evaluated according to the extent to which the endplate overlaid with presynaptic components. For each muscle sample, 500 endplates were evaluated from randomly selected visual fields. Blind acquisition and analysis were performed using coded slides from three animals for each genotype.

For CSA analysis, triceps muscles were embedded in tissue-freezing medium, snap frozen in nitrogen-cooled isopentane, and stained. A minimum of three transversal 7-μm sections were arbitrarily chosen from the middle region of each muscle and photomicrographed using AxioVision 3.1 software. The mean CSA of at least 2,000 myofibers for each genotype was analyzed with ImageJ software.

For SMN gem detection, spinal cords were isolated from mice after perfusion, incubated overnight in 4% PFA solution, and transferred overnight in 30% sucrose in PBS at 4°C. 15-μm sections from the lumbar regions (L1–L5) were dissected, and one in every five sections was processed for immunofluorescence analysis. After heat-mediated antigen retrieval (10-mM sodium citrate and 0.05% Tween 20, pH 6.0; 10 min of microwaving), sections were incubated for 3 d with pri-

mary antibodies (prepared in 2% BSA in PBS containing 0.1% Triton X-100): mouse anti-SMN (1:100; BD), goat anti-ChAT (1:200; EMD Millipore), and rabbit anti-SAM68 (1:200; Santa Cruz Biotechnology, Inc.). Sections were incubated for 2 h at room temperature with secondary antibodies: Alexa Fluor 488 donkey anti-mouse IgG (1:200; Molecular Probes), Alexa Fluor 555 donkey anti-goat IgG (1:200; Molecular Probes), and Alexa Fluor 647 donkey anti-rabbit IgG (1:200; Molecular Probes). DAPI was used for nuclear staining. Sections were examined by a confocal laser-scanning microscope (LSM700; Carl Zeiss).

### Western blot analysis

Western blot analysis was performed as previously described (Paronetto et al., 2007). The primary antibodies (1:1,000) were rabbit anti-SAM68, mouse anti-ACTIN, mouse anti-GAPDH (all from Santa Cruz Biotechnology, Inc.), mouse anti-U2AF65 (Sigma-Aldrich), and mouse anti-SMN (BD).

### Cell cultures, transfections, and cell extract preparation

Cell cultures, transfections, and sample preparation were performed by standard methods as previously described (Bielli et al., 2014). In brief, HEK293T cells were transfected with FLAG-SAM68 vector as indicated using Lipofectamine 2000 (Invitrogen).

### Biotin-RNA pull-down

Biotin-RNA pull-down experiments were performed using HEK293T cell nuclear extracts and SMN2 RNA probes in vitro synthesized from a PCR product amplified using primers (Table S1) and the plasmid PCI-SMN2 in the presence of biotin-labeled deoxynucleotide (Roche) as described previously (Pedrotti et al., 2010). Extracts were precleared for 1 h on protein A-Sepharose beads (Sigma-Aldrich) and 1 h on streptavidin-Sepharose beads (Sigma-Aldrich). Precleared extracts were then incubated with streptavidin-Sepharose beads in the presence of 0.1% BSA and biotinylated RNA probe for 2 h at 4°C under rotation. Beads were washed three times with washing buffer, and proteins were eluted in SDS sample buffer for Western blot analysis (Pedrotti et al., 2010).

### UV-CLIP assays

CLIP assays were performed as previously described (Bielli et al., 2014). In brief, dissociated brain tissue was irradiated three times on ice (100 mJ/cm<sup>2</sup>). Cell suspension was centrifuged at 4,000 rpm for 3 min, and the pellet was incubated for 10 min on ice in lysis buffer (50-mM Tris, pH 8.0, 100-mM NaCl, 1% NP-40, 1-mM MgCl<sub>2</sub>, 0.1-mM CaCl<sub>2</sub>, 0.5-mM Na<sub>3</sub>VO<sub>4</sub>, 1-mM DTT, protease inhibitor cocktail [Sigma-Aldrich], and RNase inhibitor [Promega]). Samples were briefly sonicated and incubated with DNase (RNase-free; Ambion) for 3 min at 37°C and then centrifuged at 15,000 g for 3 min at 4°C. 1 mg of extract was treated with Proteinase K for 30 min at 55°C, and RNA was purified by standard procedure (input) or diluted to 1 ml with lysis buffer and immunoprecipitated using anti-SAM68 (Santa Cruz Biotechnology, Inc.) and anti-hnRNP A1 (Santa Cruz Biotechnology, Inc.) antibodies or IgGs (negative control) in the presence of protein G magnetic Dynabeads (Novox; Life Technologies). 1,000 IU RNase I (Ambion) was added to immunoprecipitates and incubated for 2 h at 4°C under rotation. After stringent washes (Bielli et al., 2014), an aliquot (10%) was kept as a control of immunoprecipitation, while the rest was treated with 50 μg Proteinase K and incubated for 1 h at 55°C. RNA was then isolated by standard procedures.

### qPCR analyses

qPCR was performed using LightCycler 480 SYBR green I Master and the LightCycler 480 System (Roche) according to the manufacturer's instructions. For CLIP analyses, each sample was normalized with re-

spect to its input. *SMN2* RNA associated with SAM68 or hnRNP A1 is represented as fold enrichment relative to IgG samples.

### Statistical analyses

The quantitative data are expressed as the mean  $\pm$  SD or SEM, as indicated in the figure legends. Two-tailed Student's *t* test and one-way and two-way analysis of variance (ANOVA) followed by Bonferroni's multiple comparison posttest were performed using Prism 6 software (GraphPad Software). Kaplan-Meier survival data were analyzed with the log-rank test.

### Online supplemental material

Fig. S1 shows the specific binding of SAM68 to *SMN2* pre-mRNA and motor function analysis of non-SMA *Sam68*<sup>-/-</sup> mice. Fig. S2 shows the effects of *Sam68* ablation on SMN and GEMIN2 expression in SMA $\Delta$ 7 mice and supporting data for Fig. 3. Fig. S3 shows that ablation of *Sam68* ameliorates innervation of NMJs in masseter muscle. Fig. S4 documents amelioration of peripheral defects in the SMA $\Delta$ 7/*Sam68*<sup>-/-</sup> mice. Table S1 represents the list of the oligonucleotides used as PCR or qPCR primers in this study. Online supplemental material is available at <http://www.jcb.org/cgi/content/full/jcb.201502059/DC1>.

### Acknowledgments

We thank Dr. P. Bielli for fruitful discussion throughout this work and helpful suggestions, Drs. C. Compagnucci, E. Cesari, R. Busà, F. Botti, S. Carosio, L. Forcina, and C. Nicoletti for technical assistance, and Dr. F. Biamonte for discussion of the stereological data.

This work was supported by grants from the Telethon Foundation (GGP09154 and GGP14095 to C. Sette and GGP13013 to A. Musarò), Muscular Dystrophy Association (186711 to C. Sette), Associazione Italiana Ricerca sul Cancro (14581 to C. Sette), Fondazione Roma (to C. Sette), and Fondazione Santa Lucia Ricerca Corrente.

The authors declare no competing financial interests.

Submitted: 17 February 2015

Accepted: 31 August 2015

## References

Arnold, W.D., and A.H. Burghes. 2013. Spinal muscular atrophy: Development and implementation of potential treatments. *Ann. Neurol.* 74:348–362. <http://dx.doi.org/10.1002/ana.23995>

Bäumer, D., S. Lee, G. Nicholson, J.L. Davies, N.J. Parkinson, L.M. Murray, T.H. Gilligwater, O. Ansorge, K.E. Davies, and K. Talbot. 2009. Alternative splicing events are a late feature of pathology in a mouse model of spinal muscular atrophy. *PLoS Genet.* 5:e1000773. <http://dx.doi.org/http://dx.doi.org/10.1371/journal.pgen.1000773>

Biamonte, F., G. Assenza, R. Marino, M. D'Amelio, R. Panteri, D. Caruso, S. Scurati, J.G. Yague, L.M. Garcia-Segura, R. Cesa, et al. 2009. Interactions between neuroactive steroids and reelin haploinsufficiency in Purkinje cell survival. *Neurobiol. Dis.* 36:103–115. <http://dx.doi.org/10.1016/j.nbd.2009.07.001>

Bianchi, E., F. Barbagallo, C. Valeri, R. Geremia, A. Salustri, M. De Felici, and C. Sette. 2010. Ablation of the *Sam68* gene impairs female fertility and gonadotropin-dependent follicle development. *Hum. Mol. Genet.* 19:4886–4894. <http://dx.doi.org/10.1093/hmg/ddq422>

Bielli, P., R. Busà, M.P. Paronetto, and C. Sette. 2011. The RNA-binding protein Sam68 is a multifunctional player in human cancer. *Endocr. Relat. Cancer.* 18:R91–R102. <http://dx.doi.org/10.1530/ERC-11-0041>

Bielli, P., R. Busà, S.M. Di Stasi, M.J. Munoz, F. Botti, A.R. Kornblihtt, and C. Sette. 2014. The transcription factor FBI-1 inhibits SAM68-mediated BCL-X alternative splicing and apoptosis. *EMBO Rep.* 15:419–427. <http://dx.doi.org/10.1002/embr.201338241>

Bose, J.K., I.F. Wang, L. Hung, W.Y. Tarn, and C.K. Shen. 2008. TDP-43 over-expression enhances exon 7 inclusion during the survival of motor neuron pre-mRNA splicing. *J. Biol. Chem.* 283:28852–28859. <http://dx.doi.org/10.1074/jbc.M805376200>

Branchu, J., O. Biondi, F. Chali, T. Collin, F. Leroy, K. Mamchaoui, J. Makoukji, C. Pariset, P. Lopes, C. Massaad, et al. 2013. Shift from extracellular signal-regulated kinase to AKT/cAMP response element-binding protein pathway increases survival-motor-neuron expression in spinal-muscular-atrophy-like mice and patient cells. *J. Neurosci.* 33:4280–4294. <http://dx.doi.org/10.1523/JNEUROSCI.2728-12.2013>

Bricceno, K.V., P.J. Sampognaro, J.P. Van Meerbeke, C.J. Sumner, K.H. Fischbeck, and B.G. Burnett. 2012. Histone deacetylase inhibition suppresses myogenin-dependent atrogenic activation in spinal muscular atrophy mice. *Hum. Mol. Genet.* 21:4448–4459. <http://dx.doi.org/10.1093/hmg/ddc286>

Burnett, B.G., E. Muñoz, A. Tandon, D.Y. Kwon, C.J. Sumner, and K.H. Fischbeck. 2009. Regulation of SMN protein stability. *Mol. Cell. Biol.* 29:1107–1115. <http://dx.doi.org/10.1128/MCB.01262-08>

Cai, D., J.D. Frantz, N.E. Tawa Jr., P.A. Melendez, B.C. Oh, H.G. Lidov, P.O. Hasselgren, W.R. Frontera, J. Lee, D.J. Glass, and S.E. Shoelson. 2004. IKK $\beta$ /NF- $\kappa$ B activation causes severe muscle wasting in mice. *Cell.* 119:285–298. <http://dx.doi.org/10.1016/j.cell.2004.09.027>

Chen, H.H., J.G. Chang, R.M. Lu, T.Y. Peng, and W.Y. Tarn. 2008. The RNA binding protein hnRNP Q modulates the utilization of exon 7 in the survival motor neuron 2 (*SMN2*) gene. *Mol. Cell. Biol.* 28:6929–6938. <http://dx.doi.org/10.1128/MCB.01332-08>

Cho, S., and G. Dreyfuss. 2010. A degron created by *SMN2* exon 7 skipping is a principal contributor to spinal muscular atrophy severity. *Genes Dev.* 24:438–442. <http://dx.doi.org/10.1101/gad.1884910>

Ehrmann, I., C. Dalgliesh, Y. Liu, M. Danilenko, M. Crosier, L. Overman, H.M. Arthur, S. Lindsay, G.J. Clowry, J.P. Venables, et al. 2013. The tissue-specific RNA binding protein T-STAR controls regional splicing patterns of *neurexin* pre-mRNAs in the brain. *PLoS Genet.* 9:e1003474. <http://dx.doi.org/10.1371/journal.pgen.1003474>

Feng, W., A.K. Gubitz, L. Wan, D.J. Battle, J. Dostie, T.J. Golembe, and G. Dreyfuss. 2005. Gemins modulate the expression and activity of the SMN complex. *Hum. Mol. Genet.* 14:1605–1611. <http://dx.doi.org/10.1093/hmg/ddi168>

Fu, X.D., and M. Ares Jr. 2014. Context-dependent control of alternative splicing by RNA-binding proteins. *Nat. Rev. Genet.* 15:689–701. <http://dx.doi.org/10.1038/nrg3778>

Galarneau, A., and S. Richard. 2009. The STAR RNA binding proteins GLD-1, QKI, SAM68 and SLM-2 bind bipartite RNA motifs. *BMC Mol. Biol.* 10:47. <http://dx.doi.org/10.1186/1471-2199-10-47>

Hofmann, Y., and B. Wirth. 2002. hnRNP-G promotes exon 7 inclusion of *survival motor neuron* (*SMN*) via direct interaction with *Htra2*- $\beta$ 1. *Hum. Mol. Genet.* 11:2037–2049. <http://dx.doi.org/10.1093/hmg/11.17.2037>

Hofmann, Y., C.L. Lorson, S. Stamm, E.J. Androphy, and B. Wirth. 2000. *Htra2*- $\beta$ 1 stimulates an exonic splicing enhancer and can restore full-length *SMN* expression to *survival motor neuron 2* (*SMN2*). *Proc. Natl. Acad. Sci. USA.* 97:9618–9623. <http://dx.doi.org/10.1073/pnas.160181697>

Hua, Y., K. Sahashi, F. Rigo, G. Hung, G. Horev, C.F. Bennett, and A.R. Krainer. 2011. Peripheral SMN restoration is essential for long-term rescue of a severe spinal muscular atrophy mouse model. *Nature.* 478:123–126. <http://dx.doi.org/10.1038/nature10485>

Huot, M.E., G. Vogel, A. Zabaraukas, C.T. Ngo, J. Coulombe-Huntington, J. Majewski, and S. Richard. 2012. The Sam68 STAR RNA-binding protein regulates mTOR alternative splicing during adipogenesis. *Mol. Cell.* 46:187–199. <http://dx.doi.org/10.1016/j.molcel.2012.02.007>

Iascone, D.M., C.E. Henderson, and J.C. Lee. 2015. Spinal muscular atrophy: From tissue specificity to therapeutic strategies. *F1000Prime Rep.* 7:04. <http://dx.doi.org/10.12703/P7-04>

Iijima, T., K. Wu, H. Witte, Y. Hanno-Iijima, T. Glatter, S. Richard, and P. Scheiffele. 2011. SAM68 regulates neuronal activity-dependent alternative splicing of *neurexin-1*. *Cell.* 147:1601–1614. <http://dx.doi.org/10.1016/j.cell.2011.11.028>

Kashima, T., and J.L. Manley. 2003. A negative element in *SMN2* exon 7 inhibits splicing in spinal muscular atrophy. *Nat. Genet.* 34:460–463. <http://dx.doi.org/10.1038/ng1207>

Kashima, T., N. Rao, and J.L. Manley. 2007. An intronic element contributes to splicing repression in spinal muscular atrophy. *Proc. Natl. Acad. Sci. USA.* 104:3426–3431. <http://dx.doi.org/10.1073/pnas.0700343104>

Le, T.T., L.T. Pham, M.E. Butchbach, H.L. Zhang, U.R. Monani, D.D. Coovert, T.O. Gavrillina, L. Xing, G.J. Bassell, and A.H. Burghes. 2005. *SMN2*, the major product of the centromeric survival motor neuron (*SMN2*) gene, extends survival in mice with spinal muscular atrophy and associates with full-length *SMN*. *Hum. Mol. Genet.* 14:845–857. <http://dx.doi.org/10.1093/hmg/ddi078>

- Li, D.K., S. Tisdale, F. Lotti, and L. Pellizzoni. 2014. SMN control of RNP assembly: From post-transcriptional gene regulation to motor neuron disease. *Semin. Cell Dev. Biol.* 32:22–29. <http://dx.doi.org/10.1016/j.semcdb.2014.04.026>
- Ling, K.K., R.M. Gibbs, Z. Feng, and C.P. Ko. 2012. Severe neuromuscular denervation of clinically relevant muscles in a mouse model of spinal muscular atrophy. *Hum. Mol. Genet.* 21:185–195. <http://dx.doi.org/10.1093/hmg/ddr453>
- Lorson, M.A., and C.L. Lorson. 2012. SMN-inducing compounds for the treatment of spinal muscular atrophy. *Future Med Chem.* 4:2067–2084. <http://dx.doi.org/10.4155/fmc.12.131>
- Lukong, K.E., and S. Richard. 2003. Sam68, the KH domain-containing superSTAR. *Biochim. Biophys. Acta.* 1653:73–86.
- Mammucari, C., G. Milan, V. Romanello, E. Masiero, R. Rudolf, P. Del Piccolo, S.J. Burden, R. Di Lisi, C. Sandri, J. Zhao, et al. 2007. FoxO3 controls autophagy in skeletal muscle in vivo. *Cell Metab.* 6:458–471. <http://dx.doi.org/10.1016/j.cmet.2007.11.001>
- Mende, Y., M. Jakubik, M. Riessland, F. Schoenen, K. Rossbach, A. Kleinridders, C. Köhler, T. Buch, and B. Wirth. 2010. Deficiency of the splicing factor *Sfrs10* results in early embryonic lethality in mice and has no impact on full-length *SMN/Smn* splicing. *Hum. Mol. Genet.* 19:2154–2167. <http://dx.doi.org/10.1093/hmg/ddq094>
- Nurputra, D.K., P.S. Lai, N.I. Harahap, S. Morikawa, T. Yamamoto, N. Nishimura, Y. Kubo, A. Takeuchi, T. Saito, and Y. Takeshima et al. 2013. Spinal muscular atrophy: From gene discovery to clinical trials. *Ann. Hum. Genet.* 77:435–463. <http://dx.doi.org/http://dx.doi.org/10.1111/ahg.12031>
- Paronetto, M.P., T. Achsel, A. Massiello, C.E. Chalfant, and C. Sette. 2007. The RNA-binding protein Sam68 modulates the alternative splicing of *Bcl-x*. *J. Cell Biol.* 176:929–939. <http://dx.doi.org/10.1083/jcb.200701005>
- Paronetto, M.P., V. Messina, E. Bianchi, M. Barchi, G. Vogel, C. Moretti, F. Palombi, M. Stefanini, R. Geremia, S. Richard, and C. Sette. 2009. Sam68 regulates translation of target mRNAs in male germ cells, necessary for mouse spermatogenesis. *J. Cell Biol.* 185:235–249. <http://dx.doi.org/10.1083/jcb.200811138>
- Pedrotti, S., and C. Sette. 2010. Spinal muscular atrophy: A new player joins the battle for SMN2 exon 7 splicing. *Cell Cycle.* 9:3874–3879. <http://dx.doi.org/10.4161/cc.9.19.13153>
- Pedrotti, S., P. Bielli, M.P. Paronetto, F. Ciccocanti, G.M. Fimia, S. Stamm, J.L. Manley, and C. Sette. 2010. The splicing regulator Sam68 binds to a novel exonic splicing silencer and functions in *SMN2* alternative splicing in spinal muscular atrophy. *EMBO J.* 29:1235–1247. <http://dx.doi.org/10.1038/emboj.2010.19>
- Richard, S., N. Torabi, G.V. Franco, G.A. Tremblay, T. Chen, G. Vogel, M. Morel, P. Cl eroux, A. Forget-Richard, S. Komarova, et al. 2005. Ablation of the Sam68 RNA binding protein protects mice from age-related bone loss. *PLoS Genet.* 1:e74. <http://dx.doi.org/10.1371/journal.pgen.0010074>
- Ruggiu, M., V.L. McGovern, F. Lotti, L. Saieva, D.K. Li, S. Kariya, U.R. Monani, A.H. Burghes, and L. Pellizzoni. 2012. A role for SMN exon 7 splicing in the selective vulnerability of motor neurons in spinal muscular atrophy. *Mol. Cell. Biol.* 32:126–138. <http://dx.doi.org/10.1128/MCB.06077-11>
- Shababi, M., J. Habibi, H.T. Yang, S.M. Vale, W.A. Sewell, and C.L. Lorson. 2010. Cardiac defects contribute to the pathology of spinal muscular atrophy models. *Hum. Mol. Genet.* 19:4059–4071. <http://dx.doi.org/10.1093/hmg/ddq329>
- Singh, N.N., J. Seo, E.W. Ottesen, M. Shishimorova, D. Bhattacharya, and R.N. Singh. 2011. TIA1 prevents skipping of a critical exon associated with spinal muscular atrophy. *Mol. Cell. Biol.* 31:935–954. <http://dx.doi.org/10.1128/MCB.00945-10>
- Wahl, M.C., C.L. Will, and R. L uhrmann. 2009. The spliceosome: Design principles of a dynamic RNP machine. *Cell.* 136:701–718. <http://dx.doi.org/10.1016/j.cell.2009.02.009>
- West, M.J., L. Slomianka, and H.J. Gundersen. 1991. Unbiased stereological estimation of the total number of neurons in the subdivisions of the rat hippocampus using the optical fractionator. *Anat. Rec.* 231:482–497. <http://dx.doi.org/10.1002/ar.1092310411>
- Zhang, Z., F. Lotti, K. Dittmar, I. Younis, L. Wan, M. Kasim, and G. Dreyfuss. 2008. SMN deficiency causes tissue-specific perturbations in the repertoire of snRNAs and widespread defects in splicing. *Cell.* 133:585–600. <http://dx.doi.org/10.1016/j.cell.2008.03.031>